ICASSP 2026 - 2026 IEEE International Conference on Acoustics, Speech and Signal Processing (ICASSP) | 979-8-3315-6701-9/26/$31.00 ©2026 IEEE | DOI: 10.1109/ICASSP55912.2026.11461855

EVENT-DRIVEN NEUROMORPHIC NEAR-FIELD RADAR IMAGING

Ayush Jha[1,3], *Abijith Jagannath Kamath*[1], *Chandra Sekhar Seelamantula*[1]
Ch. V. Narasimha Rao[3], *Chetan Singh Thakur*[2]

[1]Department of Electrical Engineering, Indian Institute of Science, Bengaluru
[2]Department of Electronic Systems Engineering, Indian Institute of Science, Bengaluru
[3]Space Applications Center, Indian Space Research Organisation, Ahmedabad
Email: {ayushjha, abijithj, css, csthakur}@iisc.ac.in, cvnrao@sac.isro.gov.in

ABSTRACT

Multiple-input multiple-output (MIMO) synthetic aperture radar (SAR) is a high-resolution imaging modality with applications such as concealed weapon detection. MIMO SAR effectively enables increasing the aperture of the radar by virtue of mechanically scanning over an extended aperture plane. Although MIMO SAR increases the imaging resolution, it comes at the price of increased acquisition overhead. In this paper, we propose an event-driven strategy for signal acquisition in a frequency-modulated continuous-wave (FMCW) MIMO SAR using *neuromorphic encoders* in place of standard analog-to-digital converters. A neuromorphic encoder is power efficient and acquires signal-dependent measurements in an opportunistic fashion — the input signal is encoded using a sequence of events only when there is a significant change in the signal amplitude. We use neuromorphic encoders to acquire the dechirped backscattered signals and achieve signal reconstruction by exploiting sparsity in a Fourier basis. We validate the effectiveness of our technique by demonstrating high-resolution image reconstruction from real-world mmWave radar acquisitions. Such an acquisition setup reduces the data acquisition overload since no measurements are made when the backscattered signals are weak while providing accurate image reconstruction.

Index Terms— Near-field radar imaging, MIMO synthetic aperture radar, neuromorphic sampling, sparse recovery, event-driven sampling.

1. INTRODUCTION

Millimeter wave (mmWave) radar has emerged as a pivotal technology for high-resolution imaging in applications such as concealed weapon detection (CWD) [1–3], nondestructive evaluation [4], biomedical imaging [5], autonomous navigation [6], and indoor mapping [7]. Widespread adoption of mmWave radar is largely attributed to the capability of *radio frequency* (RF) waves to penetrate a wide range of materials which may be opaque to optical imaging systems. Achieving high-resolution imaging with a mmWave radar typically requires large *apertures*, generally in the range of 10 cm to 100 cm [8]. This presents challenges, particularly for portable and compact systems designed for real-time or field-based applications [9]. To address these challenges, *multiple-input multiple-output* (MIMO) transceiver arrays have been integrated in radar systems to expand the aperture and improve image resolution [10].

This work is funded by the ISRO-IISc. Space Technology Cell.

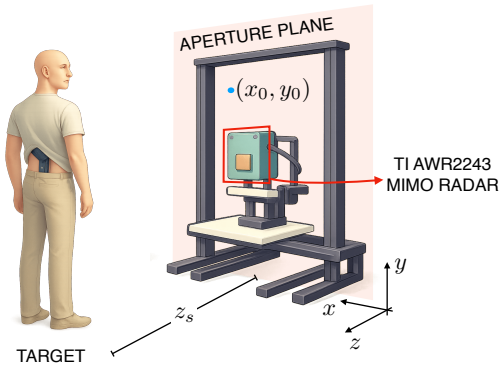

Fig. 1. Illustration of our FMCW MIMO SAR scanning setup for concealed weapon detection: A target is *illuminated* using the *Texas Instruments* (TI) AWR2243 [11] sensor mounted on a mechanical scanner platform with a predefined trajectory to increase the effective aperture.

Additionally, combining MIMO radar with synthetic aperture techniques [11, 12] — here, moving the transceivers on a predefined *scanning trajectory*, enables further reduction of hardware complexity by synthetically synthesizing larger apertures (cf. Fig. 1). Although this combination improves imaging resolution, it leads to significant data acquisition overhead. Specifically, the requirement to sample the radar signal for each transceiver position results in an extensive volume of data, which can become both inefficient and resource-intensive for large aperture systems.

1.1. Contributions and Organization of This Paper

In this paper, we consider event-driven sampling strategies to efficiently acquire signals in a MIMO *synthetic-aperture radar* (SAR). Recently, time-based/event-driven signal acquisition strategies [13–20] have demonstrated significant advantages compared to uniform Nyquist sampling. The key principle is opportunistic sampling [21], wherein, measurements are recorded only when there is a significant change in the signal. In event-driven sampling, compression in signal representation occurs at the source. Specifically, no measurements are made when the signal is weak (i.e., no targets to detect). Owing to the *sum-of-complex-exponentials* (SWCE) structure on the dechirped signal, we pose signal reconstruction as a sparse recovery problem with a Fourier basis/dictionary. On the hardware front, an event-driven *analog-to-digital converter* (ADC) has implementa-

Authorized licensed use limited to: J.R.D. Tata Memorial Library Indian Institute of Science Bengaluru. Downloaded on May 11,2026 at 05:38:25 UTC from IEEE Xplore. Restrictions apply.

tions that are power efficient [22, 23], typically by virtue of an asynchronous design where clock signals are not required. Our technique for event-driven MIMO-SAR enables high-resolution radar imaging using a power- and sample-efficient signal acquisition strategy, thus reducing the data acquisition overload. We lay out the necessary preliminaries in Section 2. We analyze signal reconstruction in Section 3. We demonstrate the technique via image reconstruction in Section 4.

2. PRELIMINARIES

We consider the monostatic signal model for FMCW radar imaging with a 2D MIMO array and neuromorphic sampling next.

2.1. Signal Model for Near-Field Radar Imaging

In 2D MIMO-SAR imaging, the objective is to recover the *reflectivity map* of a 2D scene, denoted $p(x, y)$ from indirect measurements made using a Cartesian array of co-located transceivers (monostatic mode). A transmitter at location (x_0, y_0) sends a chirp signal of the form

$$s_{\mathsf{TX}}(x_0, y_0, t) = e^{\mathrm{j}2\pi(f_0 t + \frac{1}{2}Kt^2)},$$

where f_0 denotes the carrier frequency and K denotes the chirp rate. The reflected signal is a sum of weighted and delayed copies of the transmitted signal and has the form

$$r(x_0, y_0, t) = \sum_{j=1}^{J} c_j s_{\mathsf{TX}}(t - \tau_j),$$

where J denotes the total number of reflections. The reflected signal is *dechirped* using $s^*_{\mathsf{TX}}(x_0, y_0, t)$ to obtain baseband/backscattered signal

$$\begin{aligned} s(x_0, y_0, t) &= r(x_0, y_0, t) s^*_{\mathsf{TX}}(x_0, y_0, t), \\ &= \sum_{j=1}^{J} \underbrace{c_j(x_0, y_0) e^{-\mathrm{j}2\pi f_0 \tau_j - \mathrm{j}\pi K \tau_j^2}}_{a_j} e^{\mathrm{j}2\pi K \tau_j t} = \sum_{j=1}^{J} a_j e^{\mathrm{j}2\pi f_j t}, \end{aligned} \tag{1}$$

where $f_j = 2\pi K \tau_j$ denotes the beat frequency proportional to the range of the target. The backscattered signal has a *sum of complex exponentials* (SWCE) structure. In conventional MIMO-SAR, the backscattered signal is acquired using a standard ADC.

Using the Born approximation to obtain a linearized scattering model [8], the reflectivity map is related to the backscattered data as

$$s(x_0, y_0, k) = \iint p(x, y) e^{-\mathrm{j}2kR} \, \mathrm{d}x \, \mathrm{d}y, \tag{2}$$

where $(x_0, y_0, z_0 = 0)$ represents the transceiver location, R represents the distance between the phase center of the transceiver elements and the target point, and $k(t) = \dfrac{2\pi f(t)}{c}$ denotes the wavenumber corresponding to the time-varying signal frequency $f(t) = f_0 + Kt$ [12]. Using Weyl's decomposition of a spherical wave into a sum of plane waves [2] [3], the term $e^{-\mathrm{j}2kR}$ can be approximated as:

$$e^{-\mathrm{j}2kR} \approx \iint e^{-\mathrm{j}[k_x(x-x_0)+k_y(y-y_0)+k_z z_s]} \, \mathrm{d}k_x \, \mathrm{d}k_y,$$

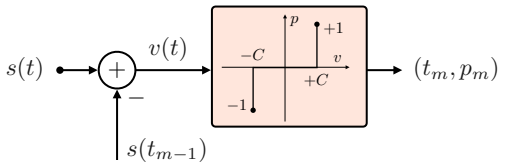

Fig. 2. Schematic of a neuromorphic encoder: the input $s(t)$ is encoded using a sequence of tuples (t_m, p_m) that denote the time-instant and polarity denoting a change in the input by C.

where z_s denotes the plane of focus. This allows representing the forward imaging model in the Fourier domain as:

$$\hat{s}(k_x, k_y, k) = \hat{p}(k_x, k_y) e^{-\mathrm{j}k_z z_s}, \tag{3}$$

where $\hat{s} = \mathsf{F}_{\mathsf{2D}}\{s\}$ and $\hat{p} = \mathsf{F}_{\mathsf{2D}}\{p\}$ denote the 2D/spatial Fourier transform of s and p, respectively, and the wavenumber components k_x, k_y, and k_z are related to the spatial dimensions x, y, and z, respectively. We use the dispersion relation [3] associated with the Weyl identity (3):

$$4k^2 = k_x^2 + k_y^2 + k_z^2.$$

The reconstructed reflectivity map at wavenumber $k = k(t)$ is given as [11, 12, 24]

$$\bar{p}(x, y, k) = \mathsf{F}^{-1}_{\mathsf{2D}} \left\{ e^{\mathrm{j}k_z z_s} \hat{s}(\cdot, \cdot, k) \right\} (x, y). \tag{4}$$

2.2. Neuromorphic Sampling

Neuromorpic sampling is an event-driven scheme for analog-to-digital conversion [25, 26]. Using a neuromorphic encoder, an input continuous-time signal is represented as a sequence of *events*, each of which are tuples containing the time-instant and polarity denoting a significant change in the signal. The acquisition is sensitive to a preset threshold $C > 0$. Fig. 2 shows an abstraction of a neuromorphic encoder using comparators. The comparator evaluates the difference between the input continuous-time signal $s(t)$ and its amplitude at the previous event instant t_{m-1} against the threshold predefined thresholds $\pm C$. When the difference exceeds $+C$, the time-instant $t = t_m$ and a positive polarity $p_m = +1$ is recorded; and conversely, when the difference falls below $-C$ the time-instant $t = t_m$ and a negative polarity $p_m = -1$ is recorded. The output of the comparators is a ternary analog signal

$$p(t) = \sum_{m \in \mathbb{N}} p_m \, \delta(t - t_m),$$

where t_m denotes the event time-instant and p_m denotes the polarity. The events are read from the ternary signal $p(t)$ using an asynchronous scheme [22, 27]. The events $e_m = (t_m, p_m)$ satisfy

$$\begin{aligned} s(t_{m+1}) - s(t_m) &= p_m C, \\ \text{where, } p_m &= \mathsf{sgn}\big(s(t_{m+1}) - s(t_m)\big), \end{aligned} \tag{5}$$

where is binary-valued in $\{-1, +1\}$.

Authorized licensed use limited to: J.R.D. Tata Memorial Library Indian Institute of Science Bengaluru. Downloaded on May 11,2026 at 05:38:25 UTC from IEEE Xplore. Restrictions apply.

3. SIGNAL RECONSTRUCTION USING SPARSE RECOVERY

Signal acquisition for high-resolution MIMO-SAR typically requires fast ADCs to acquire the backscattered signal at each transceiver. The ADC makes measurements when there are no targets to scan, as well as when the scan positions provide weak backscattered data. For each transceiver, we replace the standard ADC with a neuromorphic encoder with a constant threshold C to acquire the dechirped backscattered signal in the form of events. The in-phase and quadrature parts are encoded separately.

To recover the radar image, we begin by reconstructing the signal from events using a sparsity-based approach. We utilize the additional SWCE structure on the dechirped signal (1), i.e., the backscattered signal at (x_0, y_0) has the form:

$$s(x_0, y_0, t) = \sum_{j=1}^{J} a_j \, e^{\mathrm{j}2\pi f_j t}.$$

Using this signal model, reconstruction of the signal can be achieved by estimating the beat frequencies $\{f_j\}_{j=1}^{J}$ and weights $\{a_j\}_{j=1}^{J}$ from the sequence of events, which is a *spectral estimation problem* [28, 29]. We achieve this by exploiting sparsity.

Starting from the events and assuming the initial value is zero, we can obtain nonuniform samples of the signal considering the recursion (5) by accumulating the polarities as

$$s(x_0, y_0, t_m) = \sum_{i=1}^{m} C p_i = \sum_{j=1}^{J} a_j \, e^{\mathrm{j}2\pi f_j t_m}. \tag{6}$$

Joint estimation of the frequencies and the weights is a nonlinear problem. We consider on-grid frequency estimation by solving a sparse recovery problem. Suppose we obtain M events $\{(t_m, p_m)\}_{m=1}^{M}$ over a duration of length $T > 0$. Then, we consider the problem

$$\underset{\boldsymbol{a} \in \mathbb{C}^N}{\text{minimize}} \; \frac{1}{2} \left\| \boldsymbol{s} - \boldsymbol{P}\boldsymbol{a} \right\|_2^2, \quad \text{subject to } \|\boldsymbol{a}\|_0 \leq J, \tag{7}$$

where $s_m = s(x_0, y_0, t_m)$ and the matrix $\boldsymbol{P}$ is given as

$$\boldsymbol{P} = \begin{bmatrix} 1 & e^{\mathrm{j}2\pi\Delta f t_1} & \dots & e^{\mathrm{j}2\pi(N-1)\Delta f t_1} \\ 1 & e^{\mathrm{j}2\pi\Delta f t_2} & \dots & e^{\mathrm{j}2\pi(N-1)\Delta f t_2} \\ \vdots & \vdots & \ddots & \vdots \\ 1 & e^{\mathrm{j}2\pi\Delta f t_M} & \dots & e^{\mathrm{j}2\pi(N-1)\Delta f t_M} \end{bmatrix},$$

where $\Delta f = \dfrac{KT}{N}$, for some $N \in \mathbb{N}$. We solve the problem using *orthogonal matching pursuit* (OMP) [30–33]. Suppose $\bar{\boldsymbol{a}}$ is the estimated sparse vector, we obtain the reconstructed signal as

$$\bar{s}(x_0, y_0, t) = \sum_{n=1}^{N} \bar{a}_j \, e^{\mathrm{j}2\pi(f_0 + n\Delta f)t}.$$

Fig. 3 shows an example of the working of the reconstruction technique. We construct a sum of $J = 3$ sinusoids of frequencies 50 kHz, 150 kHz and 300 kHz, with weights 1, 0.7 and 0.5 respectively. We simulate events using a threshold $C = 0.25$. For reconstruction using OMP, we use $N = 10^3$, $\Delta f = 2.5$ kHz. The reconstructed signal is shown in Fig. 3. The signal reconstruction to error ratio is 34.88 dB, indicating accurate reconstruction.

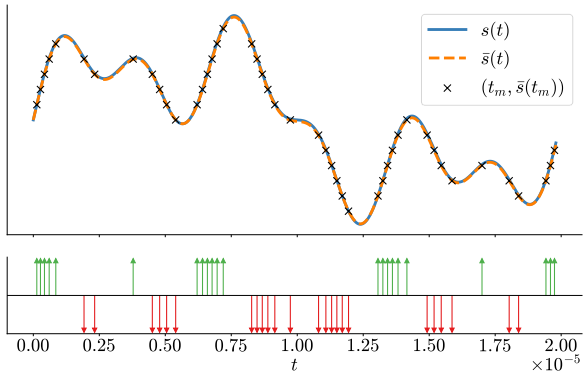

Fig. 3. Signal reconstruction using OMP: the input signal $s(t)$ is acquired in the form of events which allow computing the samples $(t_m, \bar{s}(t_m))_m$ that are the input to OMP.

4. EXPERIMENTAL RESULTS

We demonstrate event-driven FMCW MIMO-SAR on real-world measurements obtained from our experimental setup for concealed weapon detection as shown in Fig. 1. The radar is setup to illuminate a mannequin with a concealed toy gun. The corresponding optical image is shown in Fig. 4. The toy gun is concealed during radar illumination. For benchmarking, we use the reference image obtained using uniform samples. We use the peak-signal-to-noise ratio (PSNR), structural similarity index metric (SSIM) and the sampling factor defined as the ratio of total number of events acquired to the total number of uniform samples used to obtain the reference image as objective metrics for comparison.

4.1. Acquisition Setup

We construct a 2D synthetic aperture by translating the TI AWR2243 cascaded MIMO radar sensor along a parallel-track configuration using a mechanical scanner as shown in Fig. 4. The radar operates at 77 GHz with a 4 GHz bandwidth, and is equipped with 12 transmitters and 16 receivers. This configuration forms a virtual array of 86 non-overlapping MIMO elements [11], distributed along one axis with an inter-element spacing of half the wavelength to satisfy the Nyquist criterion. The effective realized aperture has a spatial dimension of 400×400 mm^2. By acquiring measurements over the 2D plane for each transmit–receive pair, the system enables

Fig. 4. Concealed weapon detection: the optical image of the scene under radar illumination in our experimental setup.

Authorized licensed use limited to: J.R.D. Tata Memorial Library Indian Institute of Science Bengaluru. Downloaded on May 11,2026 at 05:38:25 UTC from IEEE Xplore. Restrictions apply.

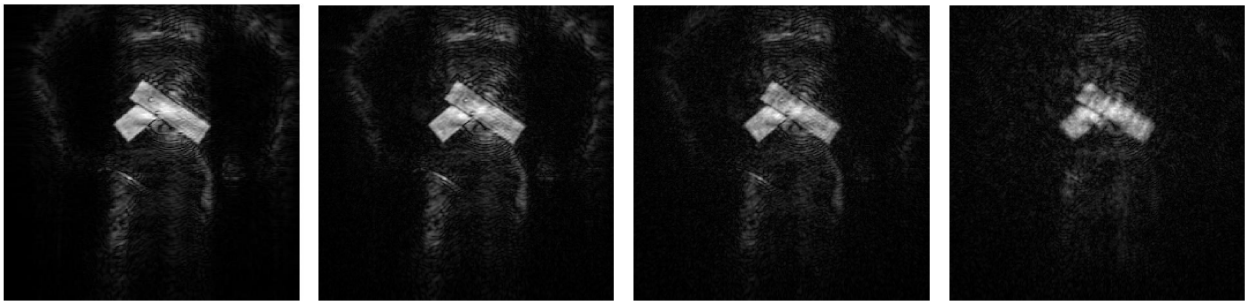

(a) Reference (b) 7%, 34.00, 0.8449, 1.64 (c) 20%, 30.06, 0.7163, 0.39 (d) 40%, 25.45, 0.5030, 0.11

Fig. 5. Radar image reconstructions obtained at $z_s = 510$ mm for different values of threshold C, along with the reference radar image obtained from the uniformly sampled backscattered signal. The numbers denote the threshold as a fraction of the dynamic range, PSNR in dB, SSIM and the sampling factor, which is the ratio of the number of events to the number of uniform samples used to obtain the reference. For a larger values of the threshold, we obtain a lower sampling factor, i.e., reduction in data acquisition, whilst continuing to obtain high-fidelity image reconstructions.

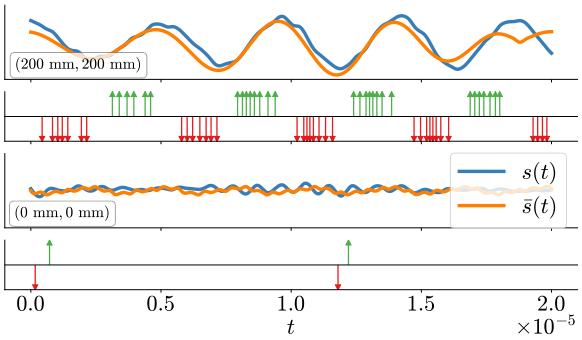

Fig. 6. Temporal streams of the backscattered data at two different locations, their corresponding acquisitions in the form of events, and their reconstructions obtained by solving OMP. The neuromorphic encoder makes few or no measurements when the backscattered signal is weak, aiding in significantly reducing the total acquired data.

high-resolution reconstruction of the target reflectivity profile. The radar is operated in time-division multiplexing (TDM) mode to ensure channel orthogonality and maximize aperture utilization.

4.2. Event Simulator

We simulate events using samples of the backscattered signal $s(x_0, y_0, t)$ measured at the Nyquist rate. We interpolate the backscattered signal to obtain a higher resolution analog-equivalent waveform and use a custom event simulator to obtain events of the form (t_m, p_m). We set the threshold C to be $7\%, 20\%$ and 40% of the maximum signal dynamic range. Fig. 6 shows the temporal waveforms of the backscattered signal at locations $(200$ mm$, 200$ mm$)$ and $(0$ mm$, 0$ mm$)$ on the aperture plane, along with the events acquired with threshold equal to 40% of the maximum signal dynamic range. The backscattered signal at (200 mm, 200 mm) is strong due to the presence of the toy gun as the target with high reflectivity. The backscattered signal at (0, 0) is weak due to the absence of any target with high reflectivity. Therefore, only a few measurements are made at location (0, 0) thereby significantly reducing the data acquisition load. The reduction in data acquired is quantified using the sampling factor.

4.3. Image Reconstruction

Given the events, we use OMP to reconstruct the backscattered signal at the Nyquist rate. Using the reconstructed backscattered signal, we recover radar images corresponding to a focal distance of $z_s = 510$ mm using (4) for a particular wavenumber $k(t)$. Next, we average the recovered frames across different wavenumbers to improve the resolution. Fig. 5 shows the reconstructed images corresponding to different thresholds C under consideration, along with the reference radar image obtained directly using the uniformly sampled backscattered signal. For a small value of the threshold C corresponding to 7% of the maximum dynamic range, the sampling factor is greater than unity. The corresponding image reconstruction has high fidelity of 34 dB. On the other hand, for a larger value of threshold corresponding to 40% of the maximum dynamic range, the sampling factor is 11%, i.e., the event-driven acquisition setup reduces the data acquisition overload by 89% compared to the conventional case using a standard ADC. Nevertheless, we continue to obtain reasonable reconstructed images of up to 25 dB PSNR.

5. CONCLUSIONS

We proposed an event-driven FMCW MIMO SAR imaging system that addresses the problem data acquisition overload. We replaced standard power hungry ADCs by power and sample efficient neuromorphic encoders to opportunistically acquire the backscattered signal in a novel event-driven MIMO-SAR imaging system. By exploiting the SWCE structure of the backscattered signal, we showed that it is possible to reconstruct the backscattered signal starting from its event representation by solving a sparse recovery problem on a Fourier basis. We used the OMP to solve the sparse recovery problem. We demonstrated the effectiveness of the technique by reconstructing radar images from real-world data obtained from our CWD setup. We demonstrated high-fidelity reconstructions across varying levels of the threshold parameter — crucially, while significantly reducing the acquisition overload. Given the successful demonstration of event-driven FMCW MIMO SAR, developing an end-to-end hardware prototype would be a fertile direction for research.

Authorized licensed use limited to: J.R.D. Tata Memorial Library Indian Institute of Science Bengaluru. Downloaded on May 11,2026 at 05:38:25 UTC from IEEE Xplore. Restrictions apply.

6. REFERENCES

[1] S. S. Ahmed, A. Schiessl, F. Gumbmann, et al., "Advanced microwave imaging," *IEEE Microw. Mag.*, vol. 13, no. 6, pp. 26–43, 2012.

[2] R. Appleby and R. N. Anderton, "Millimeter-wave and submillimeter-wave imaging for security and surveillance," *Proc. IEEE*, vol. 95, no. 8, pp. 1683–1690, 2007.

[3] D. M. Sheen, D. L. McMakin, and T. E. Hall, "Three-dimensional millimeter-wave imaging for concealed weapon detection," *IEEE Trans. Microw. Theory Techn.*, vol. 49, no. 9, pp. 1581–1592, 2001.

[4] S. Kharkovsky and R. Zoughi, "Microwave and millimeter wave nondestructive testing and evaluation — Overview and recent advances," *IEEE Instrum. Meas. Mag.*, vol. 10, no. 2, pp. 26–38, 2007.

[5] S. Di Meo, G. Matrone, M. Pasian, et al., "High-resolution mm-wave imaging techniques and systems for breast cancer detection," in *IEEE MTT-S Int. Microw. Workshop Ser. Adv. Mater. Process. RF THz Appl. (IMWS-AMP)*, 2017, pp. 1–3.

[6] M. Steinhauer, H.-O. Ruoss, H. Irion, and W. Menzel, "Millimeter-wave-radar sensor based on a transceiver array for automotive applications," *IEEE Trans. Microw. Theory Tech.*, vol. 56, no. 2, pp. 261–269, 2008.

[7] A. Kosuge, S. Suehiro, M. Hamada, and T. Kuroda, "mmWave-YOLO: A mmWave imaging radar-based real-time multiclass object recognition system for ADAS applications," *IEEE Trans. Instrum. Meas.*, vol. 71, pp. 1–10, 2022.

[8] M. I. Skolnik, "Radar handbook," *IEEE Aerosp. Electron. Syst. Mag.*, vol. 23, no. 5, pp. 41–41, 2008.

[9] M. T. Ghasr, S. Kharkovsky, R. Bohnert, B. Hirst, and R. Zoughi, "30 GHz linear high-resolution and rapid millimeter wave imaging system for NDE," *IEEE Trans. Antennas Propag.*, vol. 61, no. 9, pp. 4733–4740, 2013.

[10] D. W. Bliss and K. W. Forsythe, "Multiple-input multiple-output (MIMO) radar and imaging: degrees of freedom and resolution," in *Asilomar Conf. Signals Syst. Comput.*, 2003, vol. 1, pp. 54–59 Vol.1.

[11] M. E. Yanik, D. Wang, and M. Torlak, "Development and demonstration of MIMO-SAR mmWave imaging testbeds," *IEEE Access*, vol. 8, pp. 126019–126038, 2020.

[12] M. E. Yanik and M. Torlak, "Near-field 2-D SAR imaging by millimeter-wave radar for concealed item detection," in *IEEE Radio Wireless Symp. (RWS)*, 2019, pp. 1–4.

[13] A. A. Lazar and L. T. Tóth, "Perfect recovery and sensitivity analysis of time encoded bandlimited signals," *IEEE Trans. Circuits Syst. I*, vol. 51, no. 10, pp. 2060–2073, 2004.

[14] K. Adam, A. Scholefield, and M. Vetterli, "Sampling and reconstruction of bandlimited signals with multi-channel time encoding," *IEEE Trans. Signal Process.*, vol. 68, pp. 1105–1119, 2020.

[15] S. Rudresh, A. J. Kamath, and C. S. Seelamantula, "A time-based sampling framework for finite-rate-of-innovation signals," in *Proc. IEEE Int. Conf. Acoust., Speech, Signal Process. (ICASSP)*. IEEE, 2020, pp. 5585–5589.

[16] A.J. Kamath, S. Rudresh, and C.S. Seelamantula, "Time encoding of finite-rate-of-innovation signals," *arXiv preprint arXiv:2107.03344*, 2021.

[17] H. Naaman, S. Mulleti, and Y. C. Eldar, "FRI-TEM: Time encoding sampling of finite-rate-of-innovation signals," *IEEE Trans. Signal Process.*, vol. 70, pp. 2267–2279, 2022.

[18] A. J. Kamath and C. S. Seelamantula, "Multichannel time-encoding of finite-rate-of-innovation signals," in *Proc. IEEE Int. Conf. Acoust., Speech, Signal Process. (ICASSP)*, 2023.

[19] R. Alexandru and P. L. Dragotti, "Reconstructing classes of non-bandlimited signals from time encoded information," *IEEE Trans. Signal Process.*, vol. 68, pp. 747–763, 2019.

[20] A. J. Kamath, S. B. Patil, and C. S. Seelamantula, "DeepFRI: A deep plug-and-play technique for finite-rate-of-innovation signal reconstruction," *IEEE Trans. Signal Process.*, vol. 73, pp. 2998–3013, 2025.

[21] K. M. Guan and A. C. Singer, "Opportunistic sampling by level-crossing," in *Proc. IEEE Int. Conf. Acoust., Speech, Signal Process. (ICASSP)*. IEEE, 2007, vol. 3, pp. 1513–1516.

[22] R. Berner, C. Brandli, M. Yang, S.-C. Liu, and T. Delbruck, "A 240×180 10mw 12μs latency sparse-output vision sensor for mobile applications," in *Symposium on VLSI Circuits*, 2013, pp. C186–C187.

[23] S. Mulleti, T. Zirtiloglu, A. Tan, et al., "Power-efficient sampling: Towards low-power analog-to-digital converters," *IEEE Signal Process. Mag.*, vol. 42, no. 2, pp. 106–125, 2025.

[24] A. Jha, D. Chandrika, C. S. Seelamantula, and C. S. Thakur, "3D-Image reconstruction using MIMO-SAR FMCW radar," *arXiv preprint arXiv:2509.05977*, 2025.

[25] A. J. Kamath and C. S. Seelamantula, "Neuromorphic sampling of signals in shift-invariant spaces," *arXiv preprint arXiv:2306.05103*, 2023.

[26] A. J. Kamath and C. S. Seelamantula, "Neuromorphic sampling of sparse signals," *arXiv preprint arXiv:2310.15750*, 2023.

[27] P. Lichtsteiner, C. Posch, and T. Delbrück, "A 128 $\times$ 128 120 dB 15 μs latency asynchronous temporal contrast vision sensor," *IEEE J. Solid-State Circuits*, vol. 43, no. 2, pp. 566–576, 2008.

[28] P. Stoica and R. Moses, *Introduction to Spectral Analysis.*, Englewood Cliffs, NJ, USA: Prentice-Hall, 2000.

[29] R. Guo, Y. Zhu, and A. Bhandari, "Event-driven prony: Towards asynchronous spectral estimation," in *Proc. IEEE Int. Conf. Acoust. Speech Signal Process.*, 2025, pp. 1–5.

[30] S. G. Mallat and Z. Zhang, "Matching pursuits with time-frequency dictionaries," *IEEE Trans. Signal Process.*, vol. 41, no. 12, pp. 3397–3415, 1993.

[31] D. L. Donoho, Y. Tsaig, I. Drori, and J. Starck, "Sparse solution of underdetermined systems of linear equations by stagewise orthogonal matching pursuit," *IEEE Trans. Inf. Theory*, vol. 58, no. 2, pp. 1094–1121, 2012.

[32] J. A. Tropp and A. C. Gilbert, "Signal recovery from random measurements via orthogonal matching pursuit," *IEEE Trans. Inf. Theory*, vol. 53, no. 12, pp. 4655–4666, 2007.

[33] S. Foucart and H. Rauhut, *A Mathematical Introduction to Compressive Sensing*, Applied and Numerical Harmonic Analysis. Springer New York, 2013.

Authorized licensed use limited to: J.R.D. Tata Memorial Library Indian Institute of Science Bengaluru. Downloaded on May 11,2026 at 05:38:25 UTC from IEEE Xplore. Restrictions apply.